Formation of nanostructured porous Cu/Au surfaces: the influence of cationic sites on (electro)-catalysis

Ilija Najdovski, PR Selvakannan, Suresh K. Bhargava* and Anthony P. O'Mullane*

Received (in XXX, XXX) Xth XXXXXXXXX 20XX, Accepted Xth XXXXXXXXX 20XX
DOI: 10.1039/b000000x

The fabrication of nanostructured bimetallic materials through electrochemical routes offers the ability to control the composition and shape of the final material that can then be effectively applied as (electro)-catalysts. In this work a clean and transitory hydrogen bubble templating method is employed to generate porous Cu/Au materials with a highly anisotropic nanostructured interior. Significantly, the co-electrodeposition of copper and gold promotes the formation of a mixed bimetallic oxide surface which does not occur at the individually electrodeposited materials. Interestingly, the surface is dominated by Au(I) oxide species incorporated within a Cu_2O matrix which is extremely effective for the industrially important (electro)-catalytic reduction of 4-nitrophenol. It is proposed that an aurophilic type of interaction takes place between both oxidized gold and copper species which stabilizes the surface against further oxidation and facilitates the binding of 4-nitrophenol to the surface and increases the rate of reaction. An added benefit is that very low gold loadings are required typically less than 2 wt % for a significant enhancement in performance to be observed. Therefore the ability to create a partially oxidized Cu/Au surface through a facile electrochemical route that uses a clean template consisting of only hydrogen bubbles should be of benefit for many more important reactions.

1. Introduction

The creation of nanostructured bimetallic surfaces and nanoparticles for (electro)-catalytic applications has received significant attention due to improved properties over their single metallic counterparts. This is due to synergistic or fine tuning effects that can be observed when metals are used in combination either as alloys or when phase separated. By careful choice of composition, shape and size, improvements in important properties such as activity, selectivity and stability can be achieved.[1-3] There are many reported bimetallic combinations that benefit areas such as fuel cell electrocatalysis, gas and liquid phase heterogeneous catalysis and sensing. Quite often the most promising materials are those comprised of a significant portion of an expensive noble metal. The fabrication of materials that minimize their use would be of great benefit to the aforementioned applications. Two metals which have been investigated in detail for their (electro)-catalytic properties are nanostructured gold[4-15] and copper.[16-21] They demonstrate different activity with the latter having the drawback of being easily oxidized to inactive CuO and prone to electrodissolution.

However, copper-gold bimetallic materials have been identified as promising materials for both electrocatalysis and catalysis.[22-23] They are typically prepared by wet chemical methods such as impregnation on silica, TiO_2 and zeolites, sol-gel routes and the chemical reduction of both precursors in the presence of surfactants. Physical methods have also been reported such as implantation of copper and gold ions on silica followed by reduction with hydrogen at high temperatures and also by co-sputtering.[22] These methods can be quite involved and often require high temperatures, organic surfactants or capping agents which may be detrimental to their surface chemistry, or the use of expensive equipment. However, electrochemical methods offer a more straight forward route to creating bimetallic materials that can be achieved under ambient room temperature conditions.

The electrochemical fabrication of nanostructured metals is a burgeoning field of research as the size, shape and composition of the material can be tuned relatively easily by controlling factors such as the applied potential/current either in a constant mode or through different waveforms, concentration of precursors, electrolyte pH and time.[8,24-25] It has been demonstrated that gold can be electrodeposited in a variety of forms including spheres,[26] prisms,[27] rods,[28] spikes,[29] flowers[30] and dendrites[31] and copper in the form of spherical nanoparticles,[32] cubes,[33] wires[34] and dendrites.[35] However, the co-deposition of copper and gold has received little attention. Hayes et al demonstrated that 10-20 μm thick Cu/Au alloy films could be achieved from $KCu(CN)_2$ and $KAu(CN)_2$ in KCN,[36] however the use of cyanide precursors and electrolyte has environmental concerns. There is little information on the electrochemical formation of ordered nanostructured Cu/Au which is also expected to have interesting properties like those demonstrated by their chemically synthesized counterparts.[22]

A particularly interesting electrochemical route for the fabrication of metallic nanostructures is hydrogen bubble templating. This was first reported for copper[37-39] and tin[38] and has been extended to gold,[40-41] silver,[42-43] platinum,[44] cobalt,[45] lead,[46] palladium[47-48] and recently to bimetallic systems such as Cu/Pd,[49] Au/Pt[50] and Cu/Pt.[51] This approach creates a high electrochemically active surface area foam or honeycomb like material with the distinct advantage of using hydrogen bubbles as a clean deposition template. In the cases of copper, cobalt and silver the template has often been galvanically replaced with metals such as gold, platinum or palladium to create an active material. Significantly, this

bubble templating method involves vigorous hydrogen evolution which has been shown by Burke to create highly active surfaces of both copper[19] and gold[52-53] at metal wire electrodes through a mechanism akin to hydrogen embrittlement.[54] This results in the formation of clusters or adatoms with low lattice co-ordination on the surface with a coverage of ca. 2 %. In particular it has been suggested that these adatoms or metastable surface sites are easily oxidized to species such as $[Au_2(OH)_9]^{3-}_{ads}$[55] and $Cu^{+}_{ads}(hydr.)$[19] which have been shown to be highly active mediating species for many electrocatalytic reactions. Therefore, the complete removal or partial replacement of the porous copper scaffold with metals such as Pt and Pd in an additional process may not be required to form an active material.

It is known that partially oxidized gold or cationic gold clusters are catalytically active, with Au(I) species being of particular interest, due to aurophilic interactions which allows the creation of interesting chain or cluster like complexes[56] which influence activity.[57] Indeed there is mounting evidence that cationic gold on solid supports is more active than metallic gold for specific reactions.[58] It is also important in the case of copper where cuprous oxide has been shown to be a highly active (electro)-catalyst.[59-63] Given that Au(I) and Cu(I) are iso-electronic the possibility of forming a surface with both species is intriguing due to the possibility of aurophilic type interactions between these moieties on the surface.

In this work a hydrogen bubble template method is utilized to create a nanostructured Cu/Au honeycomb material with a low percentage of gold which under appropriate conditions consists of a surface dominated by both cationic gold and copper species which significantly impact on the industrially important electrocatalytic and catalytic reduction of 4-nitrophenol. Significantly this approach does not require either the complete removal or partial replacement of copper with metals such as Pt to create an active material. The creation of a honeycomb Cu/Au surface with both a low concentration of gold and cationic character may be of significant benefit to a whole range of important electron transfer reactions.

2. Experimental

Solutions containing $CuSO_4$, $KAuBr_4$, $HAuCl_4$, KBr and H_2SO_4 (Ajax Finechem) were used as received and made up with deionized water (resistivity of 18.2 MΩ cm) purified by use of a Milli-Q reagent deionizer (Millipore). A CH Instruments (CHI 760C) electrochemical analyzer was used for electrochemical experiments and conducted at 20 ± 2˚C. A standard three electrode configuration was used with a Ag/AgCl (aqueous 3M KCl) reference electrode; an inert graphite rod (3mm diameter, Johnson Matthey Ultra "F" purity grade) was used as a counter electrode to avoid any possible contamination from dissolution effects at the current densities employed, and copper foil (0.158 cm^2 area; 99.999% purity purchased from Goodfellow) was used as the working electrode. The copper electrodes were treated with 10 % v/v HNO_3 to remove surface oxides followed by rinsing in methanol and acetone and dried with nitrogen gas prior to use.

Electrolyte solutions were degassed with nitrogen for at least 10 min prior to electrochemical measurements and all electrocatalytic data was normalized to the geometric area of the electrode. Samples were weighed after mechanically detaching them from the Cu foil. Atomic absorption spectroscopy (AAS) results were collected on a Varian AAS spectrophotometer. X-Ray diffraction (XRD) measurements on samples removed from the Cu foil were conducted on a Bruker AXS X-ray diffraction system with an operating voltage and current of 40 kV and 40 mA with CuKα radiation. Scanning electron microscopy (SEM) images were taken on a FEI Nova SEM, with samples being thoroughly rinsed with Milli-Q water and dried with a flow of nitrogen prior to imaging. X-Ray photoelectron spectroscopy (XPS) measurements were collected with a Thermo K-Alpha XPS instrument at a pressure better than 1 x 10^{-9} torr with core levels aligned with C 1s binding energy of 285 eV. Surface enhanced Raman spectroscopy (SERS) was carried out on a Perkin-Elmer Raman Station 400 with a 785 nm excitation wavelength after samples were immersed for 1 hr in a 1 mM rhodamine B (Merck) solution and subsequently washed with water to remove any residual dye.

The reaction of 1 mM 4-nitrophenol (BDH) with 0.1 M $NaBH_4$ (Sigma Aldrich) was carried out at 20±2˚C in a beaker containing a total volume of 30 ml under stirring conditions with the sample fixed in the solution. The progress of the reaction was monitored by taking aliquots from the reaction mixture and performing UV-visible spectroscopy using a Varian (Cary 50) in a cuvette of 1 cm path length.

3. Results and Discussion

The electrochemical formation of porous bimetallic honeycomb Cu/Au can be achieved in a rapid manner from a plating bath consisting of 0.4 M $CuSO_4$ and 1.5 M H_2SO_4 containing $KAuBr_4$ at concentrations ranging from 5 to 50 mM. The samples were produced galvanostatically by applying a cathodic current density of 3 A cm^{-2} from 5 to 60 s at a copper foil working electrode. The formation of a porous interconnected honeycomb structure is dependent on both the rate of hydrogen evolution from the surface and the rate of metal electrodeposition. The evolution of bubbles initially from the surface and then from the growing deposit provide a transitory clean template over which the metal can be electrodeposited. Figure 1 shows the typical type of morphology that can be achieved using the hydrogen bubble templating method when the concentration of $KAuBr_4$ in the plating solution is increased from 0 to 20 mM while maintaining a constant $CuSO_4$ concentration. In all cases the presence of gold was confirmed by XPS and AAS analysis and quantified and discussed below. In each sample a layered structure can be observed where the pore sizes increase further away from the surface which is due to the coalescence of hydrogen bubbles. This is even more evident as a function of electrodeposition time (Figure S1) which clearly shows the gradual increase in pore sizes with time.

It is clear that the incorporation of $KAuBr_4$ has a dramatic effect on the overall pore size of the outermost layer of the film which gradually decreases from an average of 63 to 14 μm upon increasing the concentration of $KAuBr_4$ (Table 1). When the concentration of $KAuBr_4$ was increased to 50 mM the

overall honeycomb like structure collapsed at the outer layers but a high degree of porosity was maintained in the underlying layer with pore size diameters of 9 μm. Larger porous clusters were also formed over the surface without any ordered connectivity (Figure S2). It should be noted that the adherence to the underlying copper support was compromised for samples prepared using 50 mM $KAuBr_4$. It is assumed in this case that the highly porous nature of the material results in the mechanical strength of the film being compromised which results in the film breaking apart. In the following discussion samples are referred to as S-0 to S-4 as detailed in Table 1.

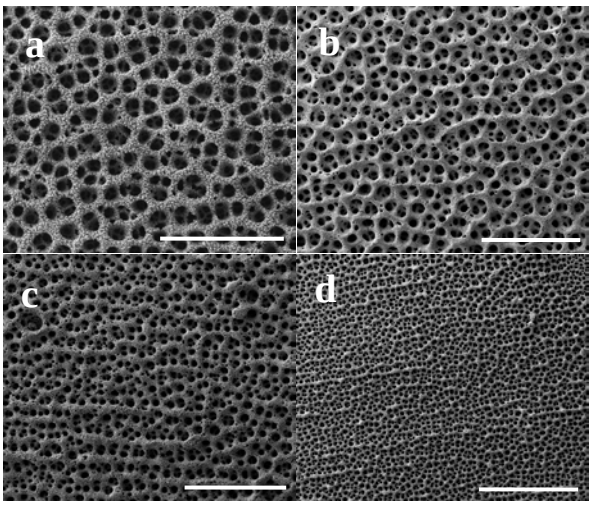

Fig. 1. SEM images of Cu/Au electrodeposited at a current density of 3 A cm^{-2} for 15 s from a solution of 0.4 M $CuSO_4$ and 1.5 M H_2SO_4 containing a) 0, b) 5, c) 10 and d) 20 mM $KAuBr_4$. Scale bar is 500 μm in all cases.

Interestingly the internal anisotropic nanostructure of the honeycomb material is also significantly altered when $AuBr_4^-$ ions are present in the plating solution (Figure 2). The highly dendritic nature of the copper only deposit (S-0) is replaced by more regular cube like structures upon using 5 or 10 mM $KAuBr_4$ (Figures 2b and c, see Figure S3a and b for higher magnification images) with diameters in the range of 500 to 800 nm for S-1 and 250 to 500 nm for S-2. A further increase to 20 mM $KAuBr_4$ (Figure 2d) results in a mixture of both block like crystallites but also thin plate like deposits (see Figure S3c for a higher magnification image). This change in microstructure may explain the gradual decrease in the pore size that is observed. It has been reported for the honeycomb copper system that the formation of closely packed dendrites with interlocking branches encourages more coalescence of hydrogen bubbles that are evolved from the surface resulting in larger pore sizes.[64] When polyethylene glycol was investigated as an additive the wall structure changed from being dendritic in nature to quite regular equiaxed grains. This significantly decreased the pore size of the material due to less coalescence of hydrogen bubbles evolving from the equiaxed grain microstructure.[64] A similar effect is likely here through changes in the morphology of the wall structure from dendritic to cube like crystals.

During the electrodeposition process Br^- ions will be liberated during the reduction of $AuBr_4^-$ and be concentrated at the electrode solution interface. To investigate whether bromide ions are influencing the growth process porous copper was synthesized from a solution containing 0.4 M $CuSO_4$, 1.5 M H_2SO_4 and 10 mM KBr. It can be seen from Figure S4 that the pore sizes increase significantly in the presence of bromide ions (compare Figure 1a and S4a). The internal wall structure also changes with the enhancement of more rod-like growth (Figure S4b). Therefore it seems that it is the presence of gold ions rather than electrochemically generated bromide ions which is dictating both the overall macroscopic pore size of the film and morphology of the wall structure. This was confirmed by fabricating a Cu/Au honeycomb structure using $HAuCl_4$ as the gold source. It is seen from Figure S5 (using 10 mM $HAuCl_4$) that cube like structures are formed which are comparable in shape to those when using 10 mM $KAuBr_4$ (Figure S3b).

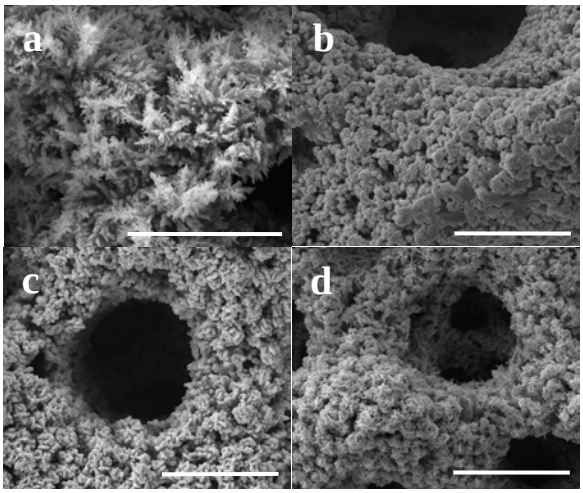

Fig. 2. Higher magnification SEM images of Cu/Au electrodeposited at a current density of 3 A cm^{-2} for 15 s from a solution of 0.4 M $CuSO_4$ and 1.5 M H_2SO_4 containing a) 0, b) 5, c) 10 and d) 20 mM $KAuBr_4$. Scale bar is 30 μm in all cases.

It was found from AAS that the bulk concentration of gold gradually increased from 0 to 2 wt % upon increasing the concentration of $KAuBr_4$ in solution (see Table 1) which is similar to the case of porous Cu/Pd reported previously.[49] The incorporation of such low concentrations of gold is shown to be extremely beneficial for both electrocatalytic and catalytic applications as discussed later which is important for reducing the use of expensive metals. However, the most interesting difference in these materials is their bulk composition and surface chemistry as a function of gold loading. Since copper and gold belong to the same cubic crystal system, there exists the possibility of forming a uniform alloy, core-shell type of alloy or phase separated copper and gold nanostructures during

Table 1. Summary of composition, pore size and crystallite size of honeycomb Cu/Au as a function of $KAuBr_4$ concentration electrodeposited from a solution containing 0.4 M $CuSO_4$ and 1.5 M H_2SO_4. Conditions employed were 3 A cm^{-2} for 15 s. Calculated d spacing of Cu(111) and Cu_2O(111) planes using Bragg equation and crystallite size using the Scherrer equation.

Sample	$KAuBr_4$ conc. (mM)	Bulk ratio Cu/Au AAS	Surface ratio Cu/Au XPS	Pore size μm	d spacing (111)		Crystallite size from (111)	
					Cu Metal (Å) 2.09	Cu_2O (Å)(2.46)	Cu Metal (nm)	Cu_2O (nm)
S-0	0	100/0	100/0	63 ± 6	2.07	2.44	37.17	35.75
S-1	5	99.5%-0.5%	99.2%-0.8%	22 ± 4	2.08	2.45	30.63	54.80
S-2	10	99.3%-0.7%	99.1%-0.9%	19 ± 4	2.07	2.44	34.3	50.29
S-3	20	98.8%-1.2%	96.8%-3.2%	14 ± 3	2.08	2.45	35.74	41.98
S-4	50	98%-2%	99.5%-0.5%	9 ± 2	2.08	2.46	38.73	40.38

electrodeposition and therefore XRD analysis of these materials was undertaken to give an insight into the nature of their crystalline phases in the bulk material (Figure 3). A copper substrate and electrochemically fabricated porous copper (S-0) were used as reference materials in order to see the effect of co-depositing gold with copper. Pure copper foil has the characteristic diffraction planes for metallic copper (04-0836), while sample S-0 has a slight amount of crystalline cuprous oxide as evidenced by the appearance of X-ray reflections typical of Cu_2O (770199) (Figure 3). However, the XRD pattern is dominated by metallic copper. Interestingly the XRD pattern of these materials show large changes when gold ions were present in the electrolyte. Significantly, the absence of metallic gold crystalline peaks suggests that there is no phase separated crystalline gold present. Also the changes in the 2theta values corresponding to metallic copper are not significant enough to suggest that metallic gold was alloyed with copper during the electro-deposition process. Rather, the addition of gold surprisingly promotes the formation of cuprous oxide which is seen from the intense Cu_2O X-ray reflections (Figure 3, S-1 to S-4). This suggests that oxidised gold species may be distributed within the cuprous oxide lattice. Since Cu(I) and Au(I) ions are iso-electronic pairs it can support the concept of uniform distribution of possibly Au(I) sprecies throughout the material. Generally, incorporation of a large atom or ion in the lattice of smaller atoms and ions, usually affects the relative intensities of different crystalline planes. This effect is observed here where at the lower surface concentrations of gold (S-1 and S-2), the relative intensities of cuprous oxide crystalline planes are stronger than the metallic copper crystalline planes (in particular when the (111) reflections are compared), while at the highest surface concentration of gold (S-3), metallic copper crystalline planes became more intense. The formation of Cu_2O is also likely to be the origin of the change in morphology of the internal wall structure of these materials from dendritic to cube like structures seen in the SEM images (Figure 2) as it is known that Cu_2O adopts this morphology quite readily under electrochemical synthesis conditions.[65-66] In particular for sample S-3 the cube like structures, indicative of Cu_2O, are no longer dominant but co-exist with plate like structures which from XRD analysis is likely to be due to the increased amount of metallic copper.

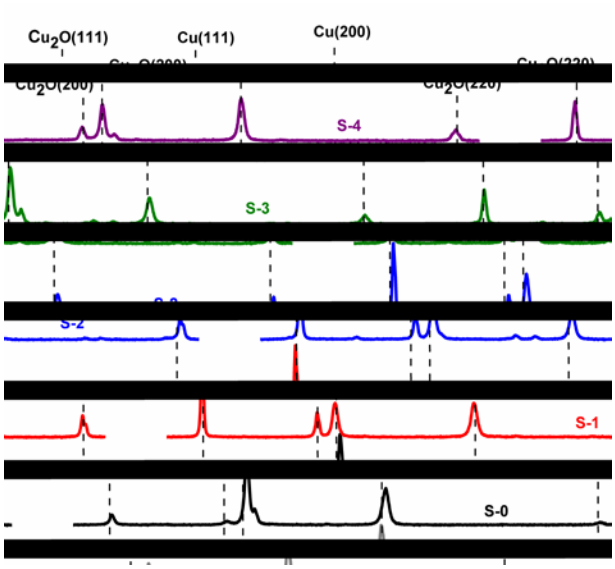

Fig. 3. Powder X-Ray diffraction patterns of copper foil, porous copper and porous copper with increasing fractions of gold.

Using the Bragg and Scherrer equations, the interplanar spacing "d" and crystallite sizes were calculated from the Cu(111) and Cu_2O(111) diffraction planes and the variation in these parameters in both systems also gives an insight into where gold has been incorporated. As shown in Table 1, there are no significant changes in the interplanar spacing of Cu_2O or Cu systems when Au ions are used in the electrochemical synthesis, however, the crystallite size of Cu_2O increases significantly when gold is incorporated into the structure with a concomitant decrease in the crystallite size of metallic copper. It is interesting to note that Cu_2O can be formed under such low pH conditions. This is most likely achieved through a localized pH change at the electrode surface. At the current densities employed here it is expected that there will be significant depletion of H^+ ions at the electrode surface which would result in a temporary alkaline environment.[67] This is expected as the potential value during the deposition is typically -2.5 V. Under these conditions the formation of oxidised species of copper and gold would be facilitated. This is analogous to the electrodeposition of many oxide materials such as ZnO which rely on such a local pH change in the vicinity of the electrode.[68]

In order to identify the oxidation state of this gold species and investigate the possibility of iso-electronic interaction between Cu(I) and Au(I) species XPS analysis was carried out. Figure 4a shows the Cu 2p7/2 core-level spectra obtained from porous copper with an increasing fraction of gold in the sample. As the gold fraction increases, there is a uniform increase in the binding energy from 932.7 to 933.8 eV. The increase in binding energy is attributed to the evolution of the oxidised form of copper on the surface due to the addition of gold. However when the concentration of gold precursors increases from 20 to 50 mM, no appreciable shift in the binding energy is observed. Hence the addition of gold in small concentrations promotes the formation of copper in a cationic state. Significantly for sample S-3 the clear emergence of a higher binding energy peak and shake up satellite peaks centred at 945 eV (Figure S6-1c) can be observed indicating the formation of CuO.[69] However, this species appears to be confined to the surface as no evidence of bulk CuO formation was observed in the XRD pattern. This is also accompanied by a significant decrease in the intensity of the Cu_2O (111) reflection compared to the Cu (111) reflection (Figure 3).

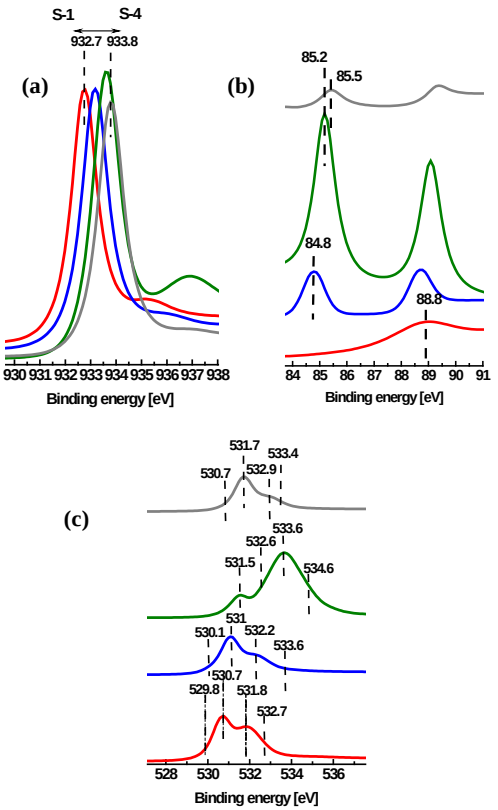

Figure 4. XPS core level spectra of (a) Cu 2p 7/2, (b) Au 4f and (c) O1s energy levels for Cu/Au samples: S-1 (–), S-2 (–), S-3 (–) and S-4 (–).

In the previous XRD discussion, we concluded that electrodepositing copper in the presence of gold led to the formation of a mixed phase containing copper metal and cuprous oxide wherein gold in a non metallic state was distributed. The high BE component of copper in their XPS spectra support the formation of cuprous oxide on the surface. If gold in a higher oxidation state is incorporated in a matrix of Cu(I) oxide, then an increase in the binding energy of the Au-4f core level should be observed in these materials. XPS spectra of the Au 4f core-level is shown in Figure 4b, which clearly supports the formation of a higher valent or cationic nature of gold because the observed binding energies in all these samples were found to be higher than the binding energy usually observed at 84.4 eV for metallic gold. A honeycomb porous gold sample was produced as reported previously by us using the hydrogen bubble templating method from an acidic solution containing $HAuCl_4$ or $KAuBr_4$[41] and the XPS Au 4f spectrum is shown in Figure S7 where a binding energy of 84.4 eV was observed which is indicative of gold in the metallic state.[70] This demonstrates that porous gold only is not in an oxidised form, but interestingly in the present case co-depositing gold and copper led to the formation of mixed metal oxide species. The possibility of liberated Br^- species created during the reduction of $KAuBr_4$ being converted to strongly oxidising species at the counter electrode such as Br_2 or BrO^- which may chemically oxidise the deposit is ruled out since this effect was not observed in both porous gold synthesised using $KAuBr_4$ as discussed or indeed porous copper electrodeposited in the presence of 10 mM KBr (see Figure S8 for a XRD pattern indicating the absence of Cu_2O). At very low concentrations of gold (S-1), a binding energy of Au 4f was observed at 88.8 eV, typical of Au(III) oxide.[71] As the concentration of gold was increased, the BE shifts to ca. 85.0 eV, which is typical of the Au (I) oxidation state.[72-73] It is known that the oxygen atoms attached to these metal ions have characteristic O 1s binding energies which generally appear around 530 to 532 eV for gold oxides[72] and 531 eV for Cu_2O.[17] Confirmation of such mixed metal oxide species also require the examination of the O 1s binding energies of these materials and is shown in Figure 4c. Interestingly the gold/copper (I) oxide species dominate the O 1s spectrum when low concentrations of gold were used (S-1 and S-2). However for sample S-3 a significant change in the O 1s spectrum is observed with a shift to higher binding energies which is typical of adsorbed hydroxyl radicals.[72] It also coincides with a significant increase in the surface concentration of gold species from < 1 % for S-1 and S-2 to > 3 % for sample S-3. Increasing the concentration of gold in the plating bath to 50 mM (S-4) results in a lower surface concentration of gold (0.5 %) which again results in the O 1s binding energies returning to lower values comparable to samples S-1 and S-2. As discussed previously this also influences the relative intensity of the Cu_2O(111) and Cu(111) planes (Figure 3) where the intensity of the former increases again and becomes slightly higher than the latter. It should be noted that there are very minor components in the range of 534 to 535 eV in the O 1s spectrum (Figure S6-2) of these materials which is due to the presence of some residual sulphate species on the surface. All XPS spectra have been fitted and the binding energies indicated in Figure 4 correlate to the peak maxima of the fitted components. These spectra are given in detail in the supporting information section (Figure S6). By considering all of these results, the as-formed material is a kind of binary metal oxide system consisting of copper (I) and gold (I) which may be stabilized through an aurophlic type of interaction between these isoelectronic species. A similar mixed oxide material was also observed in the case of porous Cu/Au electrodeposited using $HAuCl_4$. In the presence of 10 mM $HAuCl_4$, Cu_2O oxide was formed as indicated by the XRD pattern

in Figure S9a and also cationic gold as evidence by the Au 4f spectrum which gives a peak position at 85.0 eV consistent with Au(I) species (Figure S9b). The O 1S and Cu 2p 7/2 spectra (Figure S9c and d respectively) are also consistent with those measured when Cu/Au (S-2) is electrodeposited using 10 mM $KAuBr_4$ (Figure 4).

Surface enhanced Raman spectroscopy (SERS) has been shown to be a particularly sensitive technique to characterize metal surfaces. Illustrated in Figure 5 are the SERS spectra recorded for rhodamine B which was immobilised on the surface of samples S-0 to S-4. Porous copper (S-0) demonstrates reasonable SERS activity due to the highly dendritic nature of the sample which facilitates the SERS effect through localized field enhancement at the tips and between the nanogaps of the dendrites.[49,74-75] Upon introducing gold into the structure it can be seen that there is a gradual decrease in the intensity of the response. This is further support that metallic gold is not incorporated at the surface of these materials as it is inherently more SERS active than copper as shown previously for the case of honeycomb gold.[41] The formation of oxide type materials such as Cu_2O on the surface explains the decrease in intensity of the signal as semiconducting materials exhibit weaker SERS effects due to fewer free electrons compared to the case of metals.[76]

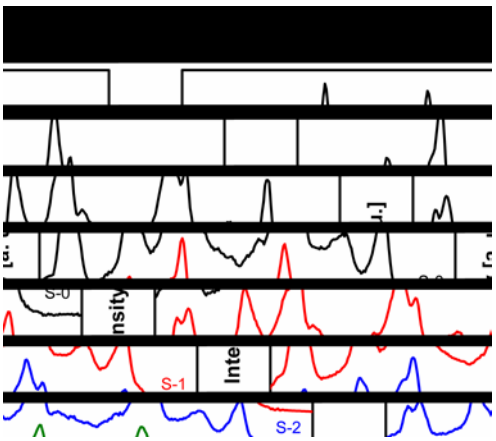

Figure 5. SERS spectra recorded for Rhodamine B immobilised on the surface of samples S-0 to S-3.

The use of a dilute amount of a second metal has been shown to be beneficial by Hutchings[77] for the carbon supported Au-M system where formulations of Au_{99}-M_1 (M = Cu, Ag and Pt) showed excellent activity for the conversion of allyl alcohol to 3-hydroxypropionic acid. However, upon increasing the amount of the second metal (M) the activity was found to decrease dramatically. In particular, it was speculated that electronic properties related to the redox properties of copper that was added to gold was responsible for the improved behavior. In the case presented here it is clear that mixed metal oxide phases are created under electrochemical conditions that are far from equilibrium. These are known to exhibit good catalytic activity but could also significantly influence the redox properties of the surface.

To test whether the formation of a bimetallic mixed metal oxide surface containing cationic sites is of benefit, the reduction of 4-nitrophenol using an excess of $NaBH_4$ was examined. This reaction was chosen as both precursors are negatively charged when they are mixed together which in principle should highly influence the reaction due to electrostatic interactions between the surface and reagents. This reaction is also of practical interest as the isolation of the product 4-aminophenol is of use to the pharmaceutical industry for the production of analgesic and antipyretic drugs.[78] The reaction can also be conveniently monitored by UV-visible spectroscopy under ambient conditions. The intense peak of 4-nitrophenol in water typically observed at 320 nm is shifted to 400 nm upon the addition of $NaBH_4$ which induces the formation of the nitrophenolate species.[79] In the absence of a catalyst this species is stable in solution where only a minor decrease in intensity of the peak at 400 nm was seen after several hours. However when honeycomb copper was introduced to the solution a gradual disappearance of this peak occurred in conjunction with the formation of a new peak at 300 nm due to the formation of 4-aminophenol (Figure 6a) as reported previously.[78-79] Interestingly, upon the introduction of sample S-1 it can be seen that the rate of reduction of the peak intensity at 400 nm increases significantly (Figure 6b) compared to the copper only sample. The kinetic rate constant for the reaction can be calculated by plotting $\ln(A_t/A_0)$ v Time (Figure 6c) and taking the slope of the linear part of the graph, where A_t is the intensity of the absorbance peak at time t and A_0 is the peak intensity at time zero. The reaction is also assumed to be first order as an excess of $NaBH_4$ is used. It can be seen that the rate increases from 5 x 10^{-3} s^{-1} to 3.3 x 10^{-2} s^{-1} upon the incorporation of a trace amount of gold species in the mixed oxide catalyst. A similar rate constant was found for S-2 (4.1 x 10^{-2} s^{-1}) whereas a significant decrease in rate (4.0 x 10^{-4} s^{-1}) was found for the highest content of gold (S-3). It should be noted that sample S-4 gave irreproducible results due to detachment of parts of the sample from the substrate.

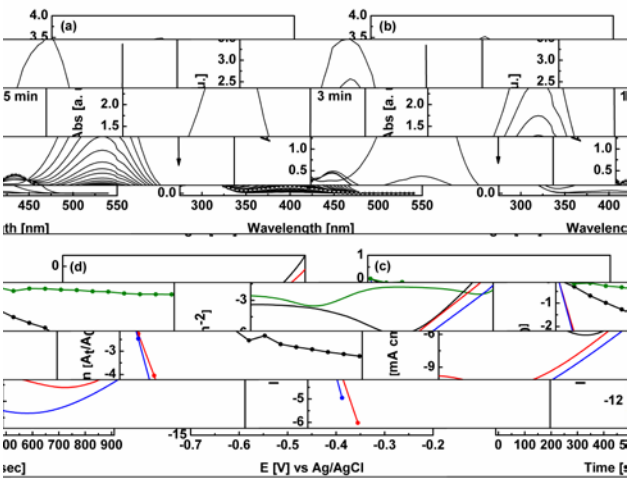

Fig. 6. Time dependent UV-vis spectra recorded for the reduction of 4-nitrophenol with $NaBH_4$ catalysed by (a) honeycomb Cu (S-0) and (b) honeycomb Cu/Au (S-1), (c) plot of $\ln(A_t/A_0)$ versus time and (d) linear sweep voltammograms recorded at 50 mV s^{-1} in 1 mM 4-nitrohenol in 0.1 M PBS for samples S-0 (–), S-1 (–), S-2 (–) and S-3 (–).

These results are also noteworthy as the conversion of 4-nitrophenol was carried out on a relatively large scale whereby a concentration of 1 mM in a total solution volume of 30 ml was undertaken. This is significantly greater than previous reports for

colloidal systems or powders which generally are investigated on the micromolar concentration range in a volume typical of a UV-visible cuvette of 3 ml. For the best sample (S-2) the amount of material electrodeposited was 1.5 mg which results in an activity factor *k* of 27.3 s^{-1} g^{-1}. Comparable trends in activity were achieved with samples electrodeposited for 5 s (S-0: 3.0 x 10^{-4} s^{-1}, S-1: 4.6 x 10^{-3} s^{-1} and S-3: 5.5 x 10^{-4} s^{-1}), however the rates were lower compared to the presented samples (Figure 6) due to less material being available for reaction (see Figure S10). The presence of oxidized gold in the sample at low concentration therefore has a significant influence on the rate of 4-nitrophenol reduction by $NaBH_4$. This was further confirmed by the addition of sample S-1 to a solution where the reaction was taking place at porous copper (S-0) only. After 11 min sample S-1 was introduced and it can be clearly seen that the rate of reaction suddenly increases with conversion achieved in 2 minutes (Figure S11).

Interestingly, the electrocatalytic reduction of 4-nitrophenol in neutral conditions followed a similar trend to the catalytic reduction reaction as shown in Figure 6d. This electrochemical reaction is also of interest as it can be either utilized as the basis of an electrochemical sensor for the detection of harmful nitrophenol species which are refractory pollutants in aqueous solution[80] or as an electrosynthesis route to important intermediates for the pharmaceutical industry as mentioned. The mechanism for the electrochemical reduction process is outlined in equations 1 and 2, where the nitro group is reduced in a two step process to a hydroxylamine.[81-82]

$$R\text{–}NO_2 + e^- \rightarrow R\text{–}NO_2^- \quad (1)$$

$$R\text{–}NO_2^- + 4H^+ + 3e^- \rightarrow R\text{–}NHOH + H_2O \quad (2)$$

It can be seen that there is an increase in the magnitude of the response over the entire potential range upon the incorporation of a low amount of gold in the samples. However a further increase in gold content (S-3) results in a significant decrease in the electrocatalytic process not only in terms of current magnitude but also the onset potential for the reaction is shifted to more negative potentials by ca. 0.25 V with respect to S-0. This behaviour trend is remarkably similar to the data presented for the catalytic reduction of 4-nitrophenol by $NaBH_4$.

Even though the reaction between 4-nitrophenol and $NaBH_4$ is thermodynamically favoured, as seen by the difference in the standard reduction potentials for 4-nitrophenol/4-aminophenol and H_3BO_3/BH_4^- of –0.76 and –1.33 V vs SHE respectively, the reaction only proceeds effectively in the presence of a catalyst. It has been shown that borohydride ion adsorption is a fast and reversible process at nanostructured metals[83] and that the reaction is dictated by the co-adsorption of 4-nitrophenolate ions which overcomes the kinetic barrier for the reaction and initiates an interfacial electron transfer reaction which is followed by desorption of neutral 4-aminophenol from the surface.[84] From these observations the origin of the significantly increased rate of 4-nitrophenol conversion to 4-aminophenol is likely to be attributed to the presence of both cationic gold and copper species on the surface. Recently it has been shown that the presence of gold cations (albeit as Au^{3+} species) on the surface of Au nanoparticles supported on Al_2O_3 significantly enhanced the rate of nitrophenol reduction by $NaBH_4$.[85] Indeed, catalytic experiments were also undertaken for the porous Cu/Pd system as reported previously by us[49] where a rate constant of 6.7 x 10^{-4} s^{-1} was observed (Figure S12). We found by XPS analysis for the Cu/Pd system that there was no indication of Pd being in an oxidized form and that more extensively oxidized copper in the form of CuO was created with no evidence of Cu_2O formation.[49] This suggests that during the electrodeposition process that the oxidation of copper in the localized alkaline environment is controlled by the co-existence of gold oxide species which prevents further oxidation to CuO through possible aurophilic type interactions. For sample S-3 the formation of hydroxyl radicals occurs on the gold surface which may prevent interaction with Cu(I) species and allow some of the Cu to be further oxidized to CuO as evidenced by the presence of shake up satellites in the Cu 2p 7/2 spectrum (Figure S6-1c) with a concomitant decrease in the intensity of the Cu_2O (111) reflection relative to the Cu (111) reflection (Figure 3). The significantly reduced rate of reaction for the Cu/Pd system clearly suggests that oxidised gold species in particular are important for the nitrophenol reduction reaction. This enhanced effect in the presence of partially oxidized gold is also supported by recent work which demonstrated that Cu_2O nanoparticles are slightly less active than Cu for the catalytic reduction of nitrophenol by $NaBH_4$.[20] It is also unlikely that size effects are a factor in influencing the rate of electron transfer as it is known that they only become apparent in the sub 5 nm range[4,86] and the cube like structures that are present in the internal wall structures are typically in the 500 nm diameter range (Figure 2) and comprised of crystallites in the 30 – 50 nm size range (Table 1).

Therefore we propose that the increased rate of reaction observed for samples S-1 and S-2 is due to the enhanced adsorption of the 4-nitrophenolate ions through an electrostatic effect where binding may occur at both the NO_2^- group and also the O^- group as shown in Scheme 1. Upon electron transfer and reaction of surface hydrogen species from adsorbed BH_4^- the neutral 4-aminophenol species desorbs from the surface. Since the amine group is an electron releasing group as compared to the strong electron withdrawing nature of the nitro group, the acidity of phenol is significantly reduced, which in turn inhibits its adsorption on a cationic surface and facilitates its removal from the surface. It should also be noted that these surface oxides are unlikely to be reduced by borohydride in solution and therefore only act as electron shuttles. Indeed the chemical synthesis of Cu_2O from Cu^{2+} precursors is often carried out using $NaBH_4$ as a reductant.[87] Gold oxide species are also quite stable and it has been shown that surface gold oxides are stable even under ultra high vacuum conditions with heating.[72] This was confirmed by exposing sample S-2 to a 0.1 M $NaBH_4$ solution for 5 min after which the sample was characterized by XRD (Figure S13). It can be seen that the peaks associated with Cu_2O are still evident and there is no appearance of metallic gold reflections. The significant decrease in the rate of reaction for sample S-3 can be related to the fact that hydroxyl radicals are adsorbed on the surface of gold as evidenced by XPS analysis which is at its highest surface concentration of all the samples investigated. This negatively charged species would inhibit the adsorption of negatively charged 4-nitrophenolate ions to the surface and

thereby limit the rate of reaction. For the electrocatalytic reactions the presence of hydroxyl radicals on the surface may also inhibit the reduction process in particular during the second step where negatively charged nitro groups are formed. Indeed it has been shown in the case of oxygen reduction on silver that adsorbed OH groups take up active sites thereby inhibiting the reduction reaction.[88]

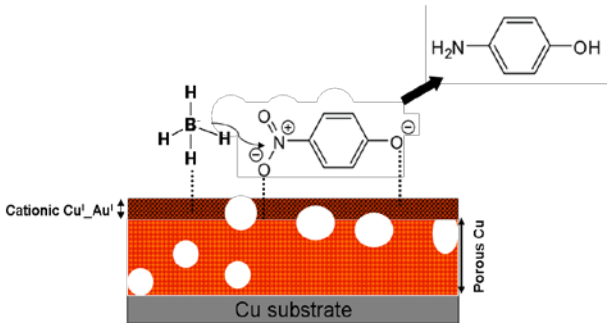

Scheme 1. Illustration of the reaction between adsorbed 4-nitrophenol and $NaBH_4$ at a cationic Cu/Au surface.

4. Conclusions

In this work we have demonstrated that honeycomb porous Cu/Au structures can be created using a hydrogen bubble templating method. The pore size of the material can be controlled by the concentration of gold salt used in the electrolyte. However, the most significant outcome is their surface chemistry properties. XPS analysis revealed that mixed metal oxide species are introduced on the surface with Au(I) species incorporated within a Cu_2O matrix material. Significantly the presence of partially oxidized gold at the surface increases the catalytic reduction of 4-nitrophenol to 4-aminophenol with $NaBH_4$ as well as its electrocatalytic reduction. The formation of this mixed oxide material may be due to aurophilic type interactions between the copper and gold iso-electronic species whereas the enhanced performance is due to better binding of 4-nitrophenol to the surface which facilitates the reaction. The major benefits of this approach is that it uses a clean transitory template that does not need removal and it minimizes the use of expensive gold where concentrations of less than 2 wt % were found to be the most effective. The creation of such active surfaces may be useful for many more electron transfer reactions that need to be catalyzed.

Acknowledgements

The authors gratefully acknowledge funding provided by the Australian Research Council (ARC) (DP 110105125) and the RMIT Microscopy and Microanalysis Facility, RMIT University for SEM and XPS facilities. AOM also acknowledges the ARC for a Future Fellowship (FT110100760).

Notes and references

School of Applied Sciences, RMIT University, GPO Box 2476V, Melbourne VIC 3001 Australia; E-mail: anthony.omullane@rmit.edu.au

[1] R. Ghosh Chaudhuri, S. Paria, *Chem Rev.*, 2012, **112**, 2373-2433.
[2] A. Cao, G. Veser, *Nat. Mater.*, 2010, **9**, 75-81.
[3] B. M. Muñoz-Flores, B. I. Kharisov, V. c. M. Jiménez-Pérez, P. Elizondo Martínez, S. T. López, *Indust. Eng. Chem. Res.*, 2011, **50**, 7705-7721.
[4] M. Haruta, N. Yamada, T. Kobayashi, S. Iijima, *J. Catal.*, 1989, **115**, 301-309.
[5] T. A. Baker, X. Liu, C. M. Friend, *Phys. Chem. Chem. Phys.*, 2011, **13**, 34-46.
[6] G. J. Hutchings, *Catalysis Today*, 2005, **100**, 55-61.
[7] C. Della Pina, E. Falletta, M. Rossi In *Catalysis*; The Royal Society of Chemistry: 2010; Vol. 22.
[8] B. J. Plowman, S. K. Bhargava, A. P. O'Mullane, *Analyst*, 2011, **136**, 5107-5119.
[9] J. Solla-Gullon, F. J. Vidal-Iglesias, J. M. Feliu, *Ann. Reports C*, 2011, **107**.
[10] L. D. Burke, *Gold Bull.*, 2004, **37**, 125-135.
[11] L. D. Burke, P. F. Nugent, *Gold Bull.*, 1998, **31**, 39-50.
[12] M. Haruta, *Faraday Discussions*, 2011, **152**.
[13] Y. Zhang, X. Cui, F. Shi, Y. Deng, *Chem Rev.*, 2011, **112**, 2467-2505.
[14] A. M. Nowicka, U. Hasse, G. Sievers, M. Donten, Z. Stojek, S. Fletcher, F. Scholz, *Angew. Chem. Int. Ed.*, 2010, **49**, 3006-3009.
[15] G. C. Bond, D. T. Thompson, *Catal. Rev.*, 1999, **41**, 319-388.
[16] H. Qiu, L. Lu, L. Xue, X. Huang, *Electrochim. Acta*, 2010, **55**, 6081-6087.
[17] D. Reyter, M. Odziemkowski, D. Belanger, L. Roue, *J. Electrochem. Soc.*, 2007, **154**, K36-K44.
[18] L. D. Burke, A. M. O'Connell, R. Sharna, C. A. Buckley, *J. Appl. Electrochem.*, 2006, **36**, 919-929.
[19] M. J. A. Shiddiky, A. P. O'Mullane, J. Zhang, L. D. Burke, A. M. Bond, *Langmuir*, 2011, **27**, 10302-10311.
[20] R. Prucek, L. Kvitek, A. Panacek, L. Vancurova, J. Soukupova, D. Jancik, R. Zboril, *J. Mater. Chem.*, 2009, **19**.
[21] A. K. Patra, A. Dutta, A. Bhaumik, *Catal. Commun.*, 2010, **11**, 651-655.
[22] C. L. Bracey, P. R. Ellis, G. J. Hutchings, *Chem. Soc. Rev.*, 2009, **38**.
[23] A. Yin, C. Wen, W.-L. Dai, K. Fan, *J. Mater. Chem.*, 2011, **21**, 8997.
[24] L. P. Bicelli, B. Bozzini, C. Mele, L. D'Urzo, *Int. J. Electrochem. Sci.*, 2008, **4**, 356-527.
[25] P. Allongue, F. Maroun, *Current Opinion in Solid State and Materials Science*, 2006, **10**, 173-181.
[26] M. S. El-Deab, T. Sotomura, T. Ohsaka, *Electrochim. Acta*, 2006, **52**, 1792-1798.
[27] Y. M. Sabri, S. J. Ippolito, A. P. O'Mullane, J. Tardio, V. Bansal, S. K. Bhargava, *Nanotechnology*, 2011, **22**, 305501.
[28] Y. Tian, H. Liu, G. Zhao, T. Tatsuma, *J. Phys. Chem. B* 2006, **110**, 23478-23481.
[29] B. Plowman, S. J. Ippolito, V. Bansal, Y. M. Sabri, A. P. O'Mullane, S. K. Bhargava, *Chem. Commun.*, 2009, 5039-5041.
[30] L. Wang, S. Guo, X. Hu, S. Dong, *Electrochem. Commun.*, 2008, **10**, 95-99.
[31] T.-H. Lin, C.-W. Lin, H.-H. Liu, J.-T. Sheu, W.-H. Hung, *Chem. Commun.*, 2011, **47**.
[32] L. Huang, E.-S. Lee, K.-B. Kim, *Coll. Surf. A*, 2005, **262**, 125-131.
[33] J. Yang, W.-D. Zhang, S. Gunasekaran, *Biosens. Bioelectron.*, 2010, **26**, 279-284.
[34] A. Keilbach, J. Moses, R. Köhn, M. Döblinger, T. Bein, *Chem. Mater.*, 2010, **22**, 5430-5436.
[35] P. Wang, D. Zhang, R. Qiu, *Appl. Surf. Sc.*, 2011, **257**, 8438-8442.
[36] A. F. Jankowski, C. K. Saw, J. F. Harper, B. F. Vallier, J. L. Ferreira, J. P. Hayes, *Thin Solid Films*, 2006, **494**, 268-273.
[37] H.-C. Shin, M. Liu, *Chem. Mater.*, 2004, **16**, 5460-5464.
[38] H. C. Shin, J. Dong, M. Liu, *Adv. Mater.*, 2003, **15**, 1610-1614.

[39] N. Nikolić, K. Popov, L. Pavlović, M. Pavlović, *J. Solid State Electrochem.*, 2007, **11**, 667-675.
[40] T. N. Huan, T. Ganesh, K. S. Kim, S. Kim, S.-H. Han, H. Chung, *Biosens. Bioelectron.*, 2011, **27**, 183-186.
[41] B. J. Plowman, A. P. O'Mullane, P. R. Selvakannan, S. K. Bhargava, *Chem. Commun.*, 2010, **46**, 9182-9184.
[42] S. Cherevko, X. Xing, C.-H. Chung, *Electrochem. Commun.*, 2010, **12**, 467-470.
[43] S. Cherevko, C.-H. Chung, *Electrochim. Acta*, 2010, **55**, 6383-6390.
[44] A. Ott, L. A. Jones, S. K. Bhargava, *Electrochem. Commun.*, 2011, **13**, 1248-1251.
[45] L. Vázquez-Gómez, E. Verlato, S. Cattarin, N. Comisso, P. Guerriero, M. Musiani, *Electrochim. Acta*, 2011, **56**, 2237-2245.
[46] S. Cherevko, X. Xing, C.-H. Chung, *Appl. Surf. Sc.*, 2011, **257**, 8054-8061.
[47] G.-M. Yang, X. Chen, J. Li, Z. Guo, J.-H. Liu, X.-J. Huang, *Electrochim. Acta*, 2011, **56**, 6771-6778.
[48] X. Xing, S. Cherevko, C.-H. Chung, *Mater. Chem. Phys.*, 2011, **126**, 36-40.
[49] I. Najdovski, P. R. Selvakannan, A. P. O'Mullane, S. K. Bhargava, *Chem. Eur. J.*, 2011, **17**, 10058-10063.
[50] J. Liu, L. Cao, W. Huang, Z. Li, *ACS Appl. Mater. Interf.*, 2011, **3**, 3552-3558.
[51] S. Cherevko, N. Kulyk, C.-H. Chung, *Nanoscale*, 2012, **4**.
[52] L. D. Burke, A. J. Ahern, A. P. O'Mullane, *Gold Bull.*, 2002, **35**, 3-10.
[53] L. D. Burke, A. P. O'Mullane, *J. Solid State Electrochem.*, 2000, **4**, 285-297.
[54] P. D. Cobden, B. E. Nieuwenhuys, V. V. Gorodetskii, V. N. Parmon, *Platinum Metals Review*, 1998, **42**, 141-144.
[55] L. D. Burke, P. F. Nugent, *Gold Bull.*, 1997, **30**, 43-53.
[56] H. Schmidbaur, A. Schier, *Chem. Soc. Rev.*, 2012, **41**, 370-412.
[57] D. J. Gorin, F. D. Toste, *Nature*, 2007, **446**, 395-403.
[58] J. C. Fierro-Gonzalez, B. C. Gates, *Chem. Soc. Rev.*, 2008, **37**.
[59] S. Song, R. Rao, H. Yang, A. Zhang, *J. Phys. Chem. C*, 2010, **114**, 13998-14003.
[60] X.-Y. Yan, X.-L. Tong, Y.-F. Zhang, X.-D. Han, Y.-Y. Wang, G.-Q. Jin, Y. Qin, X.-Y. Guo, *Chem. Commun.*, 2012, **48**.
[61] A. Paracchino, V. Laporte, K. Sivula, M. Grätzel, E. Thimsen, *Nat Mater*, 2011, **10**, 456-461.
[62] Y. Xu, H. Wang, Y. Yu, L. Tian, W. Zhao, B. Zhang, *J. Phys. Chem. C*, 2011, **115**, 15288-15296.
[63] J. B. Reitz, E. I. Solomon, *J. Am. Chem. Soc.*, 1998, **120**, 11467-11478.
[64] K. Tan, M.-B. Tian, Q. Cai, *Thin Solid Films*, 2010, **518**, 5159-5163.
[65] M. J. Siegfried, K.-S. Choi, *Angew. Chem. Int. Ed.*, 2005, **44**, 3218-3223.
[66] N. Fredj, T. D. Burleigh, *J. Electrochem. Soc.*, 2011, **158**, C104-C110.
[67] D. Nam, R. Kim, D. Han, J. Kim, H. Kwon, *Electrochim. Acta*, 2011, **56**, 9397-9405.
[68] C. V. Manzano, D. Alegre, O. Caballero-Calero, B. Alen, M. S. Martin-Gonzalez, *J. Appl. Phys.*, 2011, **110**, 043538-043538.
[69] M. F. Al-Kuhaili, *Vacuum*, 2008, **82**, 623-629.
[70] Y. Zhang, Q. Huang, Z. Zou, J. Yang, W. Vogel, H. Yang, *J. Phys. Chem. C*, 2010, **114**, 6860-6868.
[71] K. Juodkazis, J. Juodkazyte, V. Jasulaitiene, A. Lukinskas, B. Sebeka, *Electrochem. Commun.*, 2000, **2**, 503-507.
[72] J. J. Pireaux, M. Liehr, P. A. Thiry, J. P. Delrue, R. Caudano, *Surf. Sc.*, 1984, **141**, 221-232.
[73] M. P. Casaletto, A. Longo, A. Martorana, A. Prestianni, A. M. Venezia, *Surf. Interf. Anal.*, 2006, **38**, 215-218.
[74] L. Wang, H. Li, J. Tian, X. Sun, *ACS Appl. Mater. Interf.*, 2010, **2**, 2987-2991.
[75] G. Duan, W. Cai, Y. Luo, Z. Li, Y. Li, *Appl. Phys. Lett.*, 2006, **89**, 211905-211903.
[76] R.-C. Wang, C.-H. Li, *Acta Materialia*, 2011, **59**, 822-829.
[77] E. Falletta, C. Della Pina, M. Rossi, Q. He, C. J. Kiely, G. J. Hutchings, *Faraday Discussions*, 2011, **152**.
[78] Y. Lu, J. Yuan, F. Polzer, M. Drechsler, J. Preussner, *ACS Nano*, 2010, **4**, 7078-7086.
[79] F.-h. Lin, R.-a. Doong, *J. Phys. Chem. C*, 2011, **115**, 6591-6598.
[80] I. G. Casella, M. Contursi, *J. Electrochem. Soc.*, 2007, **154**, D697-D702.
[81] T. Ndlovu, O. A. Arotiba, R. W. Krause, B. B. Mamba, *Int. J. Electrochem. Sci.*, 2010, **5**, 1179-1186.
[82] D. De Souza, L. H. Mascaro, O. Fatibello-Filho, *Int. J. Anal. Chem.*, 2011, **2011**.
[83] S. Wunder, F. Polzer, Y. Lu, Y. Mei, M. Ballauff, *J. Phys. Chem. C*, 2010, **114**, 8814-8820.
[84] S. K. Ghosh, M. Mandal, S. Kundu, S. Nath, T. Pal, *Appl. Catal. A*, 2004, **268**, 61-66.
[85] H. Yazid, R. Adnan, M. A. Farrukh, S. A. Hamid, *J. Chin. Chem. Soc.*, 2011, **58**, 593-601.
[86] M. C. Saint-Lager, I. Laoufi, A. Bailly, O. Robach, S. Garaudee, P. Dolle, *Faraday Discussions*, 2011, **152**.
[87] G. Fan, F. Li, *Chem. Eng. J.*, 2011, **167**, 388-396.
[88] B. B. Blizanac, P. N. Ross, N. M. Markovic, *J. Phys. Chem. B*, 2006, **110**, 4735-4741.